Biochimica et Biophysica Acta 1807 (2011) 404–412

Contents lists available at ScienceDirect

Biochimica et Biophysica Acta

journal homepage: www.elsevier.com/locate/bbabio

Biochemical characterization of purified OmcS, a *c*-type cytochrome required for insoluble Fe(III) reduction in *Geobacter sulfurreducens*

Xinlei Qian [a,1], Tünde Mester [a,*], Leonor Morgado [b], Tsutomu Arakawa [c], Manju L. Sharma [a], Kengo Inoue [a,2], Crisjoe Joseph [d], Carlos A. Salgueiro [b], Michael J. Maroney [d], Derek R. Lovley [a]

[a] *Department of Microbiology, University of Massachusetts, Amherst, MA, USA*
[b] *Requimte-CQFB, Departamento Química, Faculdade de Ciências e Tecnologia, Universidade Nova de Lisboa, Campus Caparica, Portugal*
[c] *Alliance Protein Laboratory, Camarillo, CA, USA*
[d] *Department of Chemistry, University of Massachusetts, Amherst, MA, USA*

ARTICLE INFO

Article history:
Received 20 August 2010
Received in revised form 14 December 2010
Accepted 5 January 2011
Available online 12 January 2011

Keywords:
Geobacter sulfurreducens
C-type cytochrome
Iron reduction
Metal reduction
Humic substances

ABSTRACT

Previous studies with *Geobacter sulfurreducens* have demonstrated that OmcS, an abundant *c*-type cytochrome that is only loosely bound to the outer surface, plays an important role in electron transfer to Fe(III) oxides as well as other extracellular electron acceptors. In order to further investigate the function of OmcS, it was purified from a strain that overproduces the protein. Purified OmcS had a molecular mass of 47 015 Da, and six low-spin *bis*-histidinyl hexacoordinated heme groups. Its midpoint redox potential was −212 mV. A thermal stability analysis showed that the cooperative melting of purified OmcS occurs in the range of 65–82 °C. Far UV circular dichroism spectroscopy indicated that the secondary structure of purified OmcS consists of about 10% α-helix and abundant disordered structures. Dithionite-reduced OmcS was able to transfer electrons to a variety of substrates of environmental importance including insoluble Fe(III) oxide, Mn(IV) oxide and humic substances. Stopped flow analysis revealed that the reaction rate of OmcS oxidation has a hyperbolic dependence on the concentration of the studied substrates. A ten-fold faster reaction rate with anthraquinone-2,6-disulfonate (AQDS) (25.2 s^{-1}) was observed as compared to that with Fe(III) citrate (2.9 s^{-1}). The results, coupled with previous localization and gene deletion studies, suggest that OmcS is well-suited to play an important role in extracellular electron transfer.

1. Introduction

Members of the *Geobacteraceae* family are the predominant dissimilatory Fe(III) reducers in a diversity of subsurface environments in which Fe(III) reduction is coupled with the metabolism of organic compounds or the bioremediation of organic pollutants, radionuclides, or toxic metals [1–7]. Previous studies have demonstrated that *Geobacter* species have to establish direct contact with insoluble Fe(III) oxide for dissimilatory Fe(III) reduction [8–10]. This is in contrast to other species such as *Shewanella* and *Geothrix* species [9,10] that release compounds that act as electron shuttles between the cell surface and the Fe(III) oxides, as well as compounds that can solubilize Fe(III).

The insolubility of Fe(III) oxide requires that electrons be transferred outside the cell. It has been proposed that *c*-type cytochromes in *Geobacter* species play a key role in this extracellular electron transfer to Fe(III) based on their well-established function as electron carriers; the large number of genes encoding putative *c*-type cytochromes in *Geobacter sulfurreducens* [11,12] and *Geobacter metallireducens* [13]; and gene deletion studies that have demonstrated that several of these cytochromes are required for optimal Fe (III) reduction by *G. sulfurreducens* [14–21].

Genetic studies confirmed that the most important cytochromes in electron transfer to Fe(III) oxides are located on the outer surface of the cell including OmcB [16], a protein embedded in the outer membrane but partially exposed to the outer surface [22], and OmcS and OmcE, which are loosely attached to the cell surface [20]. OmcS is one of the most abundant cytochromes found when the proteome of Fe(III) oxide-grown cultures was compared to that of Fe(III) citrate-grown cultures, further suggesting the importance of OmcS in Fe(III) oxide reduction [23]. The finding that OmcS is associated with pili has lead to the suggestion that OmcS may facilitate the final step in Fe(III) oxide reduction after electrons are conducted out of the cell along the conductive pili [24]. OmcS may also be important for electron transfer

* Corresponding author. Present address: Department of Anesthesiology, University of Michigan, VA Medical Research Center, 2215 Fuller Road, Ann Arbor, MI 48105, USA.
E-mail address: tunde@med.umich.edu (T. Mester).
[1] Present address: Institute of Bioengineering and Nanotechnology, 31 Biopolis Way, The Nanos 04-01, Singapore 138669.
[2] Present address: Interdisciplinary Research Organization, University of Miyazaki, 5200 Kihara, Kiyotake, Japan.

0005-2728/$ – see front matter © 2011 Elsevier B.V. All rights reserved.
doi:10.1016/j.bbabio.2011.01.003

to electrodes [25] and for the reduction of humic substances [26]. Here we report on the purification and characterization of OmcS.

2. Materials and methods

2.1. Bacterial strains and culture conditions

The DLHT2215(Δ*GSU2215::kan*) (Hoa Tran, personal communication) mutant strain of *G. sulfurreducens* is a disruption mutant of GSU2215 and routinely maintained in our laboratory. This mutant was made for unrelated studies and was accidentally discovered that overproduces OmcS, which made the purification easier. It was grown under strict anaerobic conditions, as described previously [27]. Briefly, the growth medium consisted of a carbonate-buffered (1.8 g $NaHCO_3$ and 0.5 g Na_2CO_3 H_2O) minimal medium (pH 7.0) with 20 mM acetate as the electron donor and 40 mM fumarate as the electron acceptor. Cultures were grown in 500 mL of medium in 2 L bottles sitting horizontally. Cells were harvested after 5 days. The shallow cultures with larger glass surface promoted biofilm formation. OmcS (GSU2504) production reached the maximum level under these conditions.

2.2. Purification of OmcS

Cells were harvested by centrifugation at 6000 ×*g* at 4 °C for 5 min, resuspended in 50 mM Tris–HCl, pH 7.5, and subjected to a shearing force for 2 min at a low setting in a commercially available blender [20]. Sheared outer surface proteins were separated from cell debris by centrifugation at 8000 ×*g* for 10 min, and concentrated using Amicon stirred cells with a 30 kDa cutoff membrane (Millipore, MA). The sheared-off fraction was twice extracted with detergent by incubating with 5% SDS with stirring at room temperature for 20 min. The undissolved fraction was pelleted by centrifugation at 12 000 ×*g* for 20 min at 15 °C, resuspended in 50 mM Tris–HCl, pH 7.5, and incubated in a 100 °C water bath for 1 min followed with a 10 min centrifugation at 16 100 ×*g* and 4 °C. Supernatant containing solubilized OmcS was collected. Excess SDS in the collected supernatant was removed using a Detergent-OUT SDS-300 spin column (GE Biosciences, MO). Buffer was exchanged using a Zeba desalt spin column (Pierce, IL). Purified protein was stored at −20 °C.

2.3. OmcS quantification and extinction coefficient

The concentration of purified OmcS was determined with the BCA protein analysis kit (Pierce, IL). The absorbances of its absorption maxima were recorded for both reduced and oxidized OmcS standards in a series of different concentrations. The value of the molar extinction coefficient was calculated as the slope of a straight line fitted to a graph of absorbance vs. protein concentration. The reduction of OmcS with dithionite was performed under anaerobic conditions in a cuvette sealed with a rubber stopper. Concentrations of unknown samples were determined from spectrometric analysis using the extinction coefficient at 550 nm (107 800 M^{-1} cm^{-1}).

2.4. Molecular mass

The theoretical molecular mass of OmcS was calculated according to the amino acid composition (http://ca.expasy.org/tools/pi_tool.html). The molecular mass of OmcS was determined by ESI-MS under denaturing conditions (Bruker Daltonics Esquire-LC Ion trap mass spectrometer, UMass Amherst Mass Spectrometry Center).

2.5. Heme quantification

Purified cytochromes were incubated with pyridine (2.1 M) and NaOH (75 mM) in aqueous solution at room temperature for 15 min. The reducing agent sodium dithionite and the oxidizing agent potassium ferricyanide were separately added in excess to half of the cytochrome pyridine solution, resulting in pyridine ferrohemochrome and pyridine ferrihemochrome. Heme content was determined using the absorption coefficient of 11.3 mM^{-1} cm^{-1} for the absorbance of pyridine ferrohemochrome minus the absorbance of pyridine ferrihemochrome at 550 nm [28].

2.6. Electronic absorption spectroscopy

The electronic absorption spectra were acquired on a Cary 50 Bio UV–visible spectrophotometer (Varian, Australia) or an Amersham Biosciences Ultraspec 2100pro spectrophotometer (Switzerland) using a quartz optical cell. Fully reduction of the protein was achieved by adding sodium dithionite in 1 μL increments from a 2 M stock solution until full reduction was achieved.

2.7. EPR and NMR spectroscopies

For the EPR and NMR studies, OmcS solutions were prepared in 32 mM sodium phosphate buffer at pH 7.0 with NaCl (100 mM final ionic strength). Reduction of the samples was achieved by first flushing out the air from the oxidized sample with argon and then by adding sodium dithionite in 1 μL increments from a degassed 2 M stock solution to the EPR or NMR tube with a gas-tight syringe through a rubber septum. The EPR spectra were recorded with a Bruker EMX 6/1 spectrometer equipped with an Oxford Instruments ESR-900 continuous-flow helium cryostat under the following conditions: sample temperature, 4 K; microwave frequency, 9.65 GHz; microwave power, 0.6 mW; modulation amplitude, 5 G. All 1D-^{1}H NMR spectra were recorded at 400 MHz in a Bruker Avance III 400. Chemical shifts are reported in parts per million (ppm), relative to tetramethylsilane, and the proton spectra were calibrated using the water signal as internal reference. All spectra were acquired at 25 °C, by collecting 64 K data points to cover a sweep width of 60 kHz, with 48 k scans.

2.8. Circular dichroism analysis

CD spectra in the far UV, near UV and visible regions were measured on a Jasco J-715 spectropolarimeter with 1 mg/ml sample at room temperature using a 0.01, 0.2 and 0.05 cm cell, respectively. The subtracted spectra were converted to the mean residue ellipticity using the protein concentration (1 mg/ml), the path-length of the cell (0.01/0.05 cm) and the mean residue weight (105.5). Far UV CD spectrum was analyzed according to [29].

Thermal melting was done using a Jasco J-715 spectropolarimeter and a PTC-348WI temperature programmer. Temperature of the sample was controlled in a Peltier cell holder. The sample in 50 mM Tris–HCl, pH 7.5, was diluted to 0.2 mg mL^{-1} for thermal scanning at 220 nm. The 0.2 mg mL^{-1} sample was scanned at 30 °C h^{-1}. The sample was also diluted to 0.5 mg mL^{-1} for a thermal scan at 401 nm. The scan rate was set at 20 °C h^{-1}. In both spectral and melting analysis, the high tension voltage (HT[V]) data are also used to follow the absorbance (some case, light scattering) properties of the samples: HT[V] is not equal to optical density, but closely follows that parameter.

2.9. Determination of redox potential

Redox titrations of the purified form of OmcS were followed by visible spectroscopy inside an anaerobic glove box kept at <1 ppm oxygen. Following the previously described procedure [30], protein solutions in 32 mM sodium phosphate buffer with NaCl (100 mM final ionic strength) at pH 7.0 and 25 °C were used. Each redox titration was performed in both reductive and oxidative directions, using sodium dithionite and potassium ferricyanide solutions as reductant and

oxidant, respectively. To ensure a good equilibrium between the redox centers and the working electrode, a mixture of the following redox mediators was added to the solution, all at approximately 1.5 μM final concentration: phenazine methosulphate, phenazine ethosulphate, gallocyanine, methylene blue, indigo tetrasulfonate, indigo trisulfonate, indigo disulfonate, 2-hydroxy-1,4-naphthoquinone, anthraquinone-2, 6-disulfonate, anthraquinone-2-sulfonate, safranine 0, neutral red, benzyl viologen, diquat and methyl viologen. These mediators covered the potential range of −440 to +80 mV. The OmcS reduced fraction was determined by integrating the area of the α-band above the line connecting the flanking isosbestic points (543 and 562 nm in the reductive direction and 545 and 559 nm in the oxidative direction) to subtract the optical contribution of the redox mediators, as described previously [31].

2.10. Redox-activity assays

Various substrates (Au(III) chloride trihydrate, anthraquinone-2, 6-disulfonate (AQDS), U(VI) acetate; Mn(IV) oxide, Fe(III) oxide, Fe (III) citrate, potassium chromate) were prepared in anaerobic 50 mM Tris–HCl (pH 7.5) buffer. An OmcS solution in the same buffer was also prepared, reaching the concentration of 0.3 μM. OmcS was reduced by adding sodium dithionite in 1 μL increments from a 2 M stock solution until full reduction was achieved in a 1 mL quartz cuvette sealed with a rubber stopper. The reduced state of OmcS was maintained for hours without adding any oxidizing agent. Substrates were added to the fully reduced OmcS in the final concentration of 0.2 mM. The reduction and oxidation of OmcS were monitored by recording the change of absorbance at wavelengths between 250 and 600 nm using a Cary 50 Bio UV–visible spectrophotometer.

2.11. Stopped flow kinetics

All solutions used in the kinetic studies were firstly degassed with nitrogen to remove oxygen. A solution of 2.6 μM purified OmcS in 50 mM Tris–HCl, pH 7.5, was fully reduced by adding sodium dithionite in 1 μL increments from a 2 M stock solution until full reduction was achieved. The reaction of reduced OmcS (1.3 μM final concentration) with substrates anthroquinone-2,6-disulphonate (AQDS) and Fe(III) citrate was monitored using a stopped flow spectrophotometer with a rapid-scanning monochromator (RSM-1000 Olis, Inc, GA) and a 2 cm path length cell at 25 °C with an interval of 0.016 s. The stopped flow apparatus was intensively washed with oxygen-free 50 mM Tris–HCl (pH 7.5) before each run in order to maintain anaerobic conditions. OmcS was not oxidized without the substrate in the stopped flow apparatus indicating that anaerobic conditions were maintained during the experiment. UV–Vis spectra of OmcS taken before and after the reaction showed that it was fully reduced at the beginning and fully oxidized at the end of the reaction. Oxidations of OmcS by substrates such as AQDS and Fe(III) citrate were studied by monitoring the absorbance change at 550 nm. Traces obtained were fitted to an analytic expression containing one exponential term by application of non-linear iterative regression based on a least squares criterion using the Sigma Plot program. Theoretical curves were fitted to the experimental data with the Sigma Plot program.

3. Results and discussion

3.1. Purification of OmcS

As expected from previous studies [20], OmcS was the major protein in the protein fraction sheared off in the outer surface of cells. However, it was highly insoluble. The more soluble impurities were removed with a simple wash with 5% SDS in 50 mM Tris–HCl (pH 7.5). In order to solubilize OmcS it was necessary to submerge it in boiling water for 1 min in the presence of a trace amount of SDS. Solubilized OmcS was further purified from detergent and salt with a de-SDS and desalt column in order to avoid the interference from any detergent with further characterization studies.

Highly purified OmcS had an absorbance ratio of 6.7 measured at the wavelengths 410 and 280 nm corresponding to the heme groups and protein absorbances. The typical yield of OmcS obtained from 1 L of culture was 0.6 mg. Until further use, purified OmcS was kept in 50 mM Tris–HCl buffer (pH 7.5) at −20 °C. Freezing and thawing did not affect the quality of OmcS.

In order to confirm that the purified cytochrome was OmcS, the protein band shown by Coomassie staining in SDS-PAGE gel was cut and digested with trypsin for matrix-assisted laser desorption ionization (MALDI) mass spectrometry. The analysis confirmed its identity as OmcS (GSU2504) (data not shown).

3.2. Molecular mass and heme content

For precise molecular mass determination, OmcS was subjected to electrospray ionization mass spectrometry (ESI-MS) under denaturing conditions. The estimated molecular mass was 47 015 Da, which is very close to the predicted molecular mass of 46 859 Da for OmcS without its signal peptide and with the addition of the molecular mass of six heme groups (3699 Da, 616.5 Da each) [32]. Under denaturing conditions during ESI-MS, heme groups are expected to remain attached to the apoproteins with their covalent bonds. This molecular mass determination does not support the hypothesis that OmcS is anchored by its signal peptide to the outer membrane [20], and is consistent with its localization along pili [24]. However, other post-translational modifications may explain the discrepancy between the measured and theoretical molecular weight.

The similarity between the predicted and experimental molecular masses of the holoprotein indicates that OmcS has six heme groups. This was further confirmed with the pyridine hemochrome assay, which indicated a heme content of 5.7 mol of heme per mole of protein. The presence of six heme groups in a single polypeptide chain allows the cytochrome to cover a wide range of redox potential, interact with different redox partners and/or to simultaneously transfer more than one electron (see below).

3.3. UV–visible spectroscopy

The oxidized form of OmcS has a Soret band at 406 nm and a broad band at 528 nm (Fig. 1). Upon reduction with sodium dithionite, the reduced protein shows the Soret, β, and α bands at 417, 520 and 550 nm, respectively. These spectral features are typical of hexacoordinated low-spin hemes [33]. The molar extinction coefficients of these peaks are summarized in Table 1. In low-spin *c*-type cytochromes containing hemes with His-Met axial coordination, a small band at 695 nm can be detected in the oxidized form [34]. Analysis of spectra of the ferricytochrome OmcS provided no evidence for the presence of a methionine as an axial ligand (see inset in Fig. 1).

3.4. Circular dichroism analysis

OmcS was isolated from an insoluble fraction using SDS, a strong detergent, meaning that the enzyme structure may have been altered. Circular dichroism (CD) is a simple spectroscopic technique for assessing the structural integrity of proteins. CD analysis was thus performed to demonstrate the folded structure of the protein. Fig. 2A shows the near UV CD spectrum of oxidized OmcS, which reflects the environments of aromatic residues (4 Trp, 22 Tyr and 12 Phe in 409 amino acid residues). Their CD signals typically appear around 280–300 nm for Trp, 270–290 nm for Tyr and 250–270 m for Phe. Although the CD intensity is strong in this wavelength range, there appears to be no fine structures due to these aromatic groups. The number of

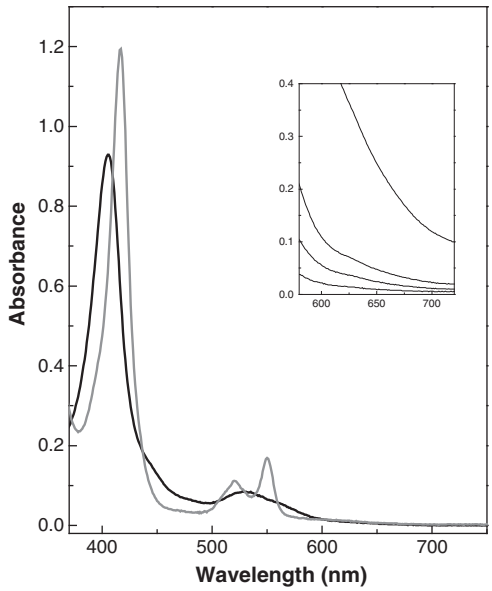

Fig. 1. Electronic absorption spectra of OmcS. Black and gray lines correspond to the oxidized and reduced form of OmcS, respectively. Expansions of the oxidized electronic absorption spectra (580 to 720 nm) obtained with different OmcS concentrations (1.6, 4.6, 9.3 and 49.7 μM, from bottom to the top) are indicated in the inset.

aromatic amino acids in OmcS is within the range of normal proteins. This may be in part due to the use of short path-length cell (0.2 cm) for 1 mg/ml protein solution. Under the normal condition, 1 cm cell is used for that protein concentration. This in turn means that the observed CD in this wavelength range comes from heme groups.

Fig. 2B shows the far UV CD spectrum. While substantial uncertainty exists due to large noise, two shoulders around 208 and 220 nm indicate presence of α-helix. The secondary structure analysis based on Greenfield and Fasman [35] and neural algorism [29] indicates that OmcS contains about 10% α-helix and abundant disordered structures.

Fig. 2C shows the visible spectrum of OmcS. While the absorbance spectrum (lower panel, expressed as high tension voltage, HT[V]) shows a single peak at 408 nm, the CD spectrum is split into two peaks (400 and 426 nm), indicating that the chromophore is in two different structures. The split is not due to two different chemical species, as the sample has one absorbance peak. Thus, the observed split of the CD peak into two peaks implies that the chromophores are in two different environments.

The thermal stability is usually used to confirm the folded structure, as unfolded structure normally shows either no or a broad melting. Thus, the melting of purified OmcS was monitored at 220 nm, which reflects changes in the secondary structure, and at 401 nm to monitor heme environments. Fig. 3A shows the change in CD signal (upper panel) and absorbance signal (lower panel) with temperature. It appears that the CD signal at 220 nm first decreases at 52 °C and then increases at 65 °C (see Fig. 3B for expanded view). The absorbance (HT[V]) data shows a gradual increase above 45 °C, suggesting that aggregation occurs prior to significant melting. This

Table 1
Absorption peaks of OmcS in the visible region of the electronic spectra and respective molar extinction coefficient.

	Peaks in the electronic absorption spectra (nm)	Molar extinction coefficient (M^{-1} cm^{-1})
Oxidized form	528	46000
	406	424400
Reduced form	550	107800
	520	67200
	417	487800

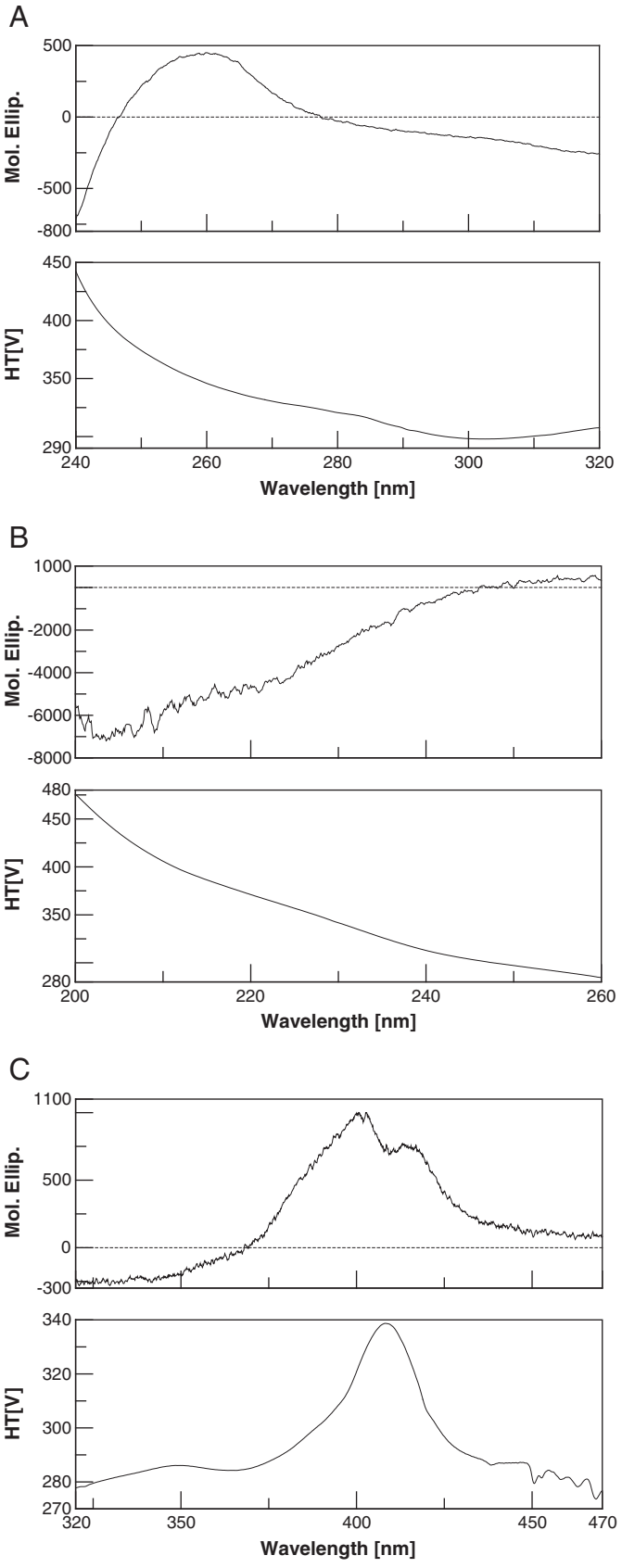

Fig. 2. Near UV (A), far UV (B) and visible (C) circular dichroism spectra of OmcS at room temperature. Conditions are detailed in Materials and methods.

aggregation makes it difficult to assess the end temperature of melting.

Fig. 3C shows the change at 401 nm, one of the two peaks observed in the visible spectrum. The CD signal begins to decrease around 65 °C and appears to plateau around 82 °C. The CD signal at 401 nm approaches zero upon melting, indicating that the hemes are exposed to the solvent due to unfolding of the protein. The absorbance increases around 45 °C, similarly to the change observed at 220 nm, indicating aggregation of the protein. By comparing the thermal scan of OmcS at 401 and 220 nm, a similar melting temperature can be observed, which indicates that secondary structure and heme environments undergo conformational changes simultaneously at 65–82 °C. This cooperative melting is a clear indication of folded structure of the protein.

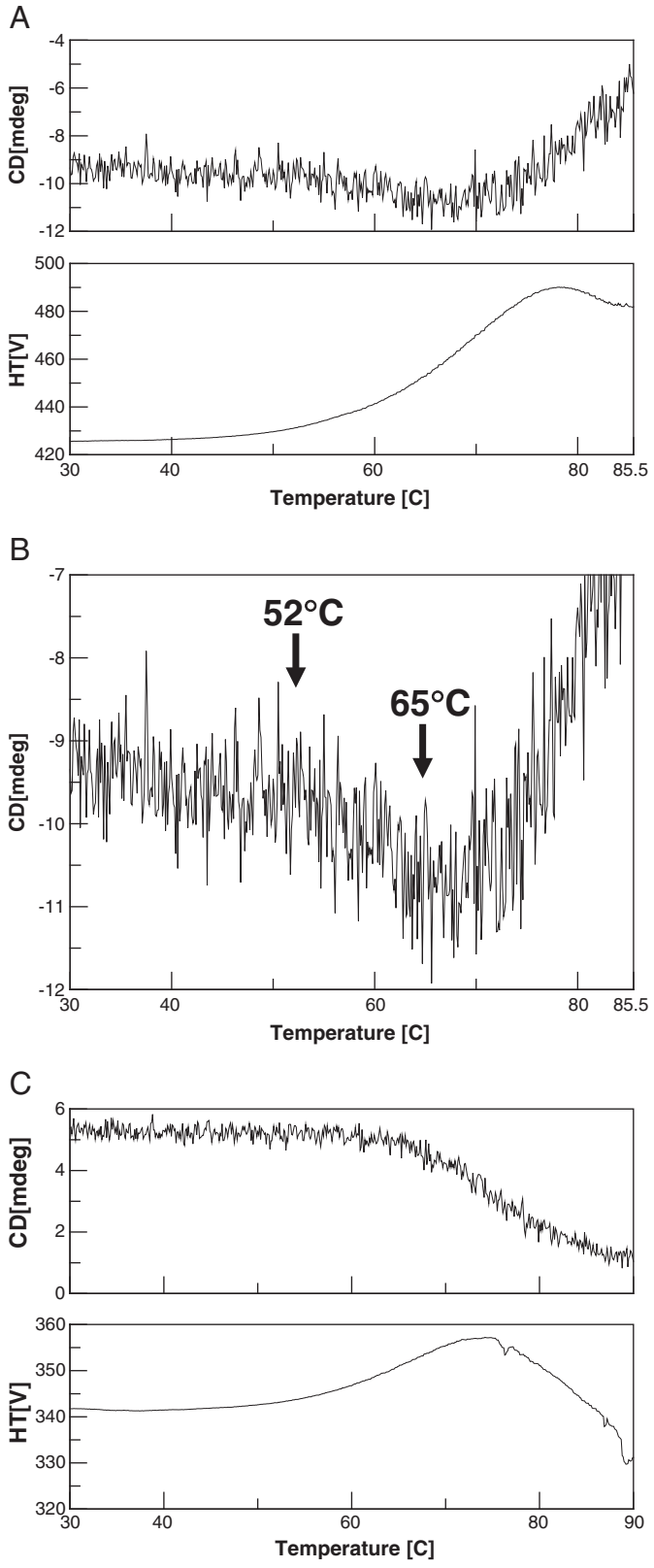

Fig. 3. Thermal melting of reduced OmcS monitored at 220 nm at a scan rate of 30 °C h^{-1} (A), or at 401 nm at the scan rate of 20 °C h^{-1} (C). CD data of the scan at 220 nm were expanded in panel B.

3.5. EPR and NMR spectroscopies

The combined use of EPR and NMR spectroscopies on cytochrome OmcS samples aimed to elucidate the spin state of the hemes and their axial coordination. The EPR spectrum of cytochrome OmcS in the oxidized form (Fig. 4) showed a rhombic EPR signal with a positive feature at $g=2.94$ (g_1), a derivative feature at 2.25 (g_2) and a very broad negative feature at 1.5 (g_3). This spectrum also showed broad features in the g_1 and g_2 regions, which might result from multiple contributions of the six heme groups. The observed g_1, g_2 and g_3 signals are characteristic of low-spin hexacoordinated heme groups with $S=1/2$. A very small signal at g-value 6.02, typical of high-spin hemes ($S=5/2$), was also detected. However, the intensity of this signal is extremely low, representing less than 1% of the total EPR heme signal intensity. This signal is in general observable even for low-spin heme proteins and represents a vestigial denaturation that occurs in the freezing of the EPR tube. The EPR spectrum of the reduced OmcS (data not shown) indicates that the spin state of the hemes is integer, however the distinction between spin states $S=0$ or $S=2$ cannot be obtained from EPR. To elucidate this, 1D-^{1}H NMR spectra of cytochrome OmcS in the fully oxidized and reduced forms were acquired (Fig. 5). The spectral regions of the heme proton signals are quite distinct for cytochromes containing high- or low-spin hemes. In the oxidized state, the NMR spectra of high-spin cytochromes show extremely broad signals above 40 ppm, which typically correspond to the heme methyls. In contrast, the low-spin heme methyl signals are mainly found in the region 8–35 ppm. Similarly, the reduced 1D-^{1}H NMR spectra of high- and low-spin cytochromes are also quite distinct. High-spin cytochromes show wider spectral regions (typically from −15 up to 30 ppm) and the heme methyl signals can be detected in the low-field region of the spectrum [35]. In contrast, the spectral widths of a reduced low-spin cytochrome are much narrow (typically from −5 to 11 ppm) [36]. In this case, the heme methyl signals are confined to the region 5–3 ppm. The OmcS NMR signals cover the regions −3 to 35 ppm and 0 to 11 ppm in the oxidized and reduced ^{1}H-NMR spectra, respectively (Fig. 5). In the fully oxidized spectrum several signals with three proton intensity are observed in the range 8–35 ppm, which correspond to the heme methyl signals. Overall, the NMR spectral features indicated that all heme groups in the cytochrome OmcS are low-spin. Thus, from the NMR studies it can be concluded that all the

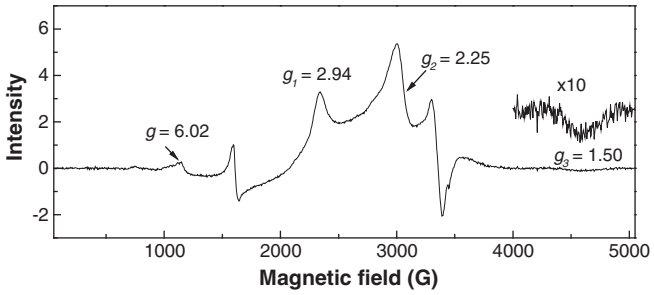

Fig. 4. EPR spectrum of oxidized OmcS and correspondent g-values. An expansion (10×) of the broad signal at g-value 1.5 is indicated.

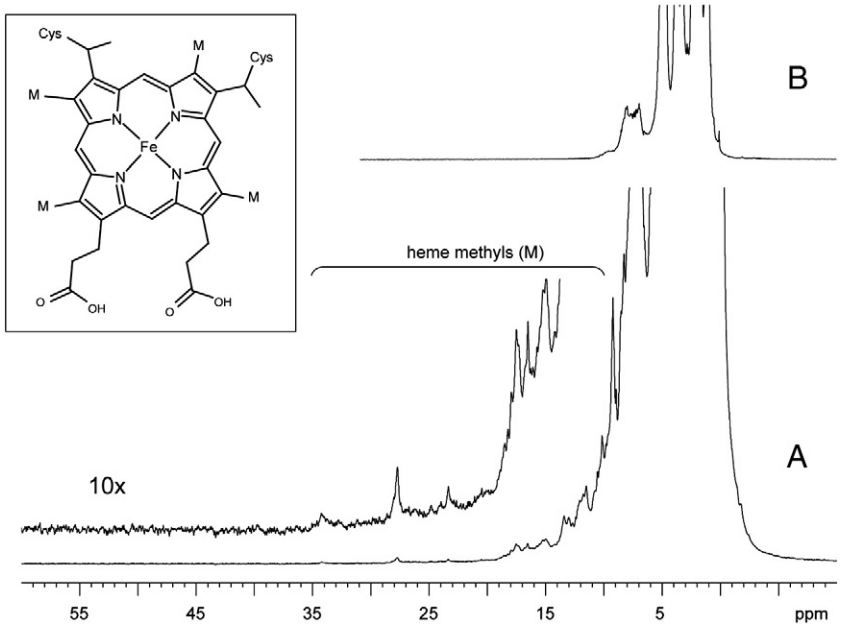

Fig. 5. 1D-^{1}H NMR spectra of the oxidized (A) and reduced (B) cytochrome OmcS. The inset indicates a diagram of a *c*-type heme. The typical chemical shift regions of the heme substituents used as fingerprints to identify the heme spin-state(s) are indicated in the reduced and in the expansion (10×) of the oxidized spectra.

OmcS heme groups are low-spin in both the oxidized ($S=1/2$) and reduced ($S=0$) forms.

The 1D-^{1}H NMR OmcS reduced spectrum further supports the result obtained with electronic absorption spectroscopy in relation to the axial coordination of the heme groups. Indeed, axially methionine-coordinated hemes display a very well-defined pattern in the low-frequency region of the reduced ^{1}H-NMR spectrum that includes a three-proton intensity peak at approximately −3 ppm, and up to four resolved one-proton intensity peaks [34,37]. In the reduced spectrum of OmcS this pattern is clearly absent, which unequivocally shows that heme groups of OmcS are not axially coordinated by a methionine residue.

3.6. Redox potential determination

The reduction potential of OmcS was determined by electrochemical redox titration (Fig. 6). The reductive and oxidative curves are superimposable, indicating that under these experimental conditions the protein can reversibly cycle between the fully reduced and fully oxidized states. The E_{app} value (i.e., the point at which the oxidized and reduced fractions are equal) at pH 7.0 was −212 mV. The redox curve spans over a large range of reduction potentials (−360 to −40 mV) and the experimental points deviate from an $n=1$ Nernst curve shown in Fig. 6 by the dashed line. This observation points to a non-equivalence of the redox centers, which is expected for a multiredox protein with six heme groups. The low reduction potential values covered by the OmcS redox curve are also compatible with *bis*-histidinyl heme groups [34].

3.7. Redox-activity of OmcS

G. sulfurreducens is able to reduce various metals and humic substances, which have relevance in biogeochemical redox cycles and environmental bioremediation of toxic organic compounds and metals [38]. The low midpoint redox potential of OmcS suggested that it will react with a wide range of electron acceptors. The reducing capability of the purified OmcS was tested with a variety of soluble and insoluble electron acceptors, which may be the natural substrates of OmcS or have relevance to environmental bioremediation. Various substrates (Table 2) were added under anaerobic conditions and the oxidation of OmcS was monitored at wavelengths between 500 and 600 nm by the disappearance of α and β bands, characteristics of reduced cytochromes. All of the substrates tested were able to oxidize OmcS. This experiment was not designed to evaluate in detail the kinetics of electron acceptor reduction, but it was apparent that the soluble substrates, with the exception of gold, instantaneously oxidized the reduced OmcS whereas reactions with insoluble substrates were much slower. OmcS attached to the Fe(III) oxide as well as to the gold precipitates that formed as the result of gold reduction. After the redox reaction with Fe(III) oxide or gold, a portion of substrate and OmcS precipitated together to the bottom of the cuvette, significantly lowering the intensities of the absorbance of the Soret, α and β bands of OmcS. The ability of OmcS to associate with Fe

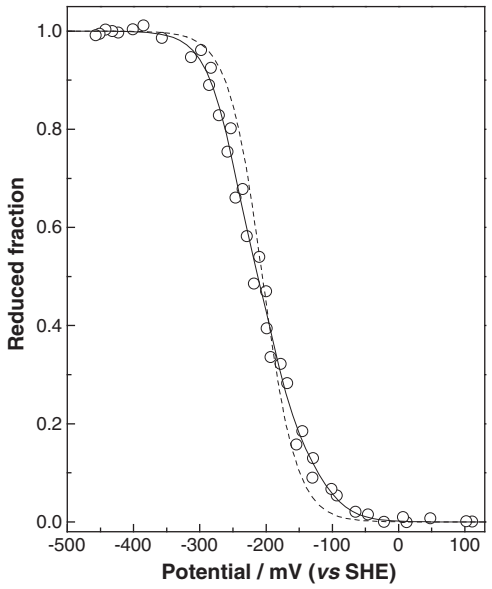

Fig. 6. Redox titration of OmcS followed by visible spectroscopy at 25 °C and pH 7.0. Experimental points are represented with open circles. The continuous line indicates the fitting to a model with six sequential one electron Nernst equations. The dashed line represents a Nernst curve for a six-electron reduction step with a midpoint potential of −212 mV.

Table 2
List of substrates that can be reduced by OmcS.

	Significance	References
Soluble substrates		
Fe(III) citrate	Model substrate for chelated Fe(III)	[38]
U(VI)	Environmental bioremediation biological uranium ore formation	[40]
Cr(VI)	Environmental bioremediation	[41]
Au(III)	Biological gold ore formation	[41]
AQDS	Model compound for humics	[42]
Humic substances	Natural substrate and redox mediator	[42]
Insoluble substrates		
Fe(III) Oxide	Most abundant Fe(III) source in subsurface environment, biological magnetite formation, geochemical iron redox cycle	[38,39]
Mn(IV) Oxides	Geochemical manganese redox cycle	[38]

(III) oxide could play an important role in electron transfer to this important insoluble electron acceptor and warrants further investigation.

3.8. Stopped flow kinetics

Mechanisms for reduction of potential physiological electron acceptors were further evaluated with stopped flow kinetic techniques performed under anaerobic conditions. Fe(III) citrate and anthraquinone-2,6-disulfonate (AQDS) serve as models for chelated metals and humic substances, respectively [39,42]. OmcS was reduced prior to the stopped flow experiment and showed high stability. Series of concentrations of Fe(III) citrate and AQDS were selected to be consistent with pseudo-first-order conditions. The analysis assumes that after rapid mixing of reduced OmcS with a large excess of substrate, that there is a rapid equilibrium and that electron transfer to substrate is irreversible:

$$\mathrm{OmcS_{red}} + \mathrm{substrate_{ox}} \overset{K_d}{\leftrightarrow} \mathrm{OmcS_{red}}$$

$$==== \mathrm{substrate_{ox}} \overset{k}{\leftrightarrow} \mathrm{OmcS_{ox}} + \mathrm{substrate_{red}}$$

The oxidation of OmcS was monitored through its α-band absorption at 550 nm, which decreases upon oxidation (Fig. 7). The reaction rates were calculated based on the rate of disappearance of the band at 550 nm, attributed to $\mathrm{OmcS_{red}}$. There was no substrate interference at this wavelength and the traces obtained followed a pseudo-first order kinetics. The traces were fitted with a single exponential equation ($A = A_0 e^{(-kt)}$) in order to obtain the observed reaction rate constant (k_{obs}).

When the observed rate constants were plotted as the function of the substrate concentration, a hyperbolic dependence of rate constants was observed for both substrates (Fig. 8). This indicates that the reduction of these substrates is the result of a reaction that consists of more than one step. The kinetic parameters were calculated by fitting the plotted k_{obs} data versus the corresponding substrate concentrations in Fig. 8 with the Michaelis–Menten equation (Table 3). The rate constant k for AQDS reduction is ten-fold higher than that of Fe(III) citrate reduction. The dissociation constants (K_d) for both substrates showed no statistical difference.

This significant difference in rate constants for the reduction of two soluble electron acceptors could not be attributed to differences in redox potentials of the two substrates because Fe(III) citrate has a more positive redox potential (−14 mV) [43] than that of AQDS (−184 mV) [44].

Further examination of the traces of OmcS oxidation with Fe(III) citrate or AQDS (Fig. 7) revealed that the two traces are somewhat different. The oxidation of OmcS by Fe(III) citrate occurs more uniformly than with AQDS where the oxidation of OmcS by AQDS can be divided into two phases, starting with a faster initial phase and ending with a slower phase. This two-phase, pre-steady-state kinetic pattern was proposed for the oxidation of outer membrane cytochromes, MtrC and OmcA from *Shewanella oneidensis*, by Fe(III) chelated with citrate, EDTA, or NTA [43]. Modeling the oxidation of OmcS by AQDS as a two-phase reaction, $A = A_0 e^{-k1t} + A_0 e^{-k2t}$, yielded a fit that, statistically, was as good as a single-phase reaction model. However, the fit for a two-phase reaction model with Fe(III) citrate was poor. Plotting the k_1 and k_2 for a two-phase reaction with AQDS versus substrate concentration, also showed hyperbolic dependency of the concentration of the redox partner with rate constants of 50.7 and 3.6 s^{-1}, respectively. The dissociation constants for the fast and slow phases were determined as 121 and 106 μM AQDS, respectively. The biphasic traces showed an approximately ratio of 5:1 between the

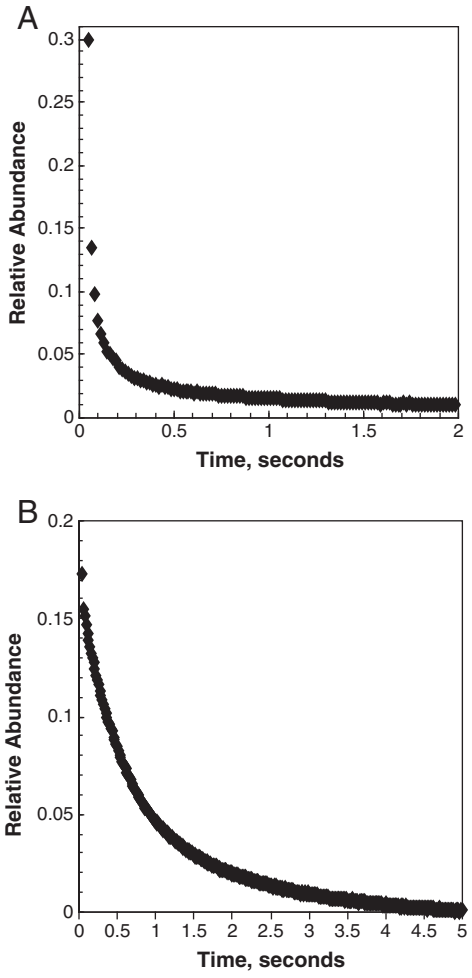

Fig. 7. Kinetic traces of OmcS oxidation by 0.125 mM AQDS (A) and 0.125 mM Fe(III) citrate (B) monitored at the wavelength of 550 nm with a stopped flow apparatus.

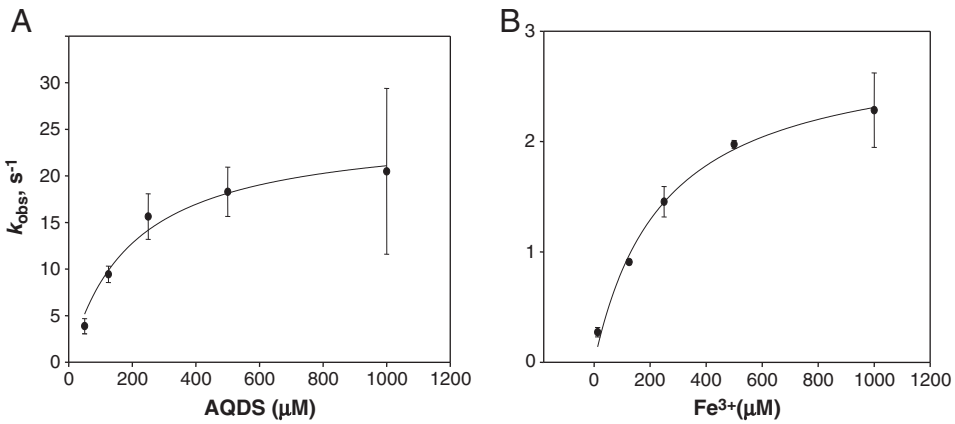

Fig. 8. Dependence of the pseudo-first order rate constants of OmcS oxidation on the concentration of AQDS (A) and Fe(III) citrate (B). Each data point represents the mean values of at least three determinations in a single experiment. The data was fitted (continuous line) using the equation of $k_{obs} = k/(1 + K_d/[S])$.

fast and slow components. One may speculate that five of the heme groups are faster oxidized than the last one. However, to test this hypothesis structural data is necessary.

A potential explanation for the possible two-phase reaction of AQDS with OmcS is that OmcS contains six hemes, which might cluster into two or more distinct or overlapping groups separated by redox potentials or different amino acid environments, as observed in other cytochromes [45,46]. In this case, the redox partners could react with two groups of hemes with different redox potential, resulting in a slower and a faster reaction. The only indication of two potentially different clusters of heme groups present in OmcS comes from the CD spectrum at visible wavelength, which exhibits a split peak and may therefore indicate different heme environments. The biphasic behavior might also be explained by the presence of two or more reaction sites with different accessibilities to the redox centers. The conformation of cytochromes may be altered by the degree of oxidation within one molecule [47], resulting in an initial fast and a subsequent slow reaction as the oxidation of cytochromes progresses, as was observed in the case of cytochrome P450 [48]. This explanation would be more consistent with the different transient state kinetic patterns of OmcS oxidation with the two very different redox partners such as Fe(III) citrate and AQDS, which may bind differently to the potential reaction sites. In order to determine whether the monophasic or the biphasic pre-steady-state kinetics of OmcS oxidation by AQDS represents a more realistically description of the mechanism, further structural and kinetic studies are necessary.

4. Implications

This is the first biochemical study of one of the *c*-type cytochromes that appear to be loosely associated with the outer-surface of *G. sulfurreducens* and may have the opportunity to establish direct contact with extracellular electron acceptors. The results demonstrate that OmcS is a promiscuous redox protein that is able to donate electrons to a wide variety of electron acceptors. This capability may explain, at least in part, why *G. sulfurreducens* can use several metals, humics and humics-related compounds as terminal electron acceptors. However, transient state kinetics studies demonstrated that there are differences in the reaction rates of reduction of different substrates, which cannot be explained simply by the redox potentials of the substrate. Further study of the structure of OmcS may yield more insight into this phenomenon. Comparative structural studies with other outer surface *c*-type cytochromes [20,24,49] may provide insights into the factors leading to their different functions.

Table 3
Pre-steady state kinetic parameters for oxidization of reduced OmcS by AQDS and Fe (III) citrate. The standard deviation values are indicated in parenthesis.

Substrate	k (s^{-1})	K_d (μM)
AQDS	25.2 (2.0)	194 (44.4)
Fe(III) citrate	2.9 (0.2)	246 (43.0)

Acknowledgements

This research was supported by the Office of Science (BER), U. S. Department of Energy, Cooperative Agreement No. DE-FC02-02ER63446. This work was also supported by project grant PTDC/BIA-PRO/74498/2006 from FCT (Portugal). L.M. was supported by FCT doctoral grant SFRH/BD/37415/2007. We acknowledge LabRMN at FCT-UNL and Rede Nacional de RMN for access to the facilities. Rede Nacional de RMN is supported with funds from FCT, Projecto de Re-equipamento Científico, Portugal.

References

[1] R.T. Anderson, H.A. Vrionis, I. Ortiz-Bernad, C.T. Resch, P.E. Long, R. Dayvault, K. Karp, S. Marutzky, D.R. Metzler, A. Peacock, D.C. White, M. Lowe, D.R. Lovley, Stimulating the *in situ* activity of *Geobacter* species to remove uranium from the groundwater of a uranium-contaminated aquifer, Appl. Environ. Microbiol. 69 (2003) 5884–5891.
[2] D.R. Bond, D.E. Holmes, L.M. Tender, D.R. Lovley, Electrode-reducing microorganisms that harvest energy from marine sediments, Science 295 (2002) 483–485.
[3] D.R. Bond, D.R. Lovley, Electricity production by *Geobacter sulfurreducens* attached to electrodes, Appl. Environ. Microbiol. 69 (2003) 1548–1555.
[4] J.R. Lloyd, D.R. Lovley, Microbial detoxification of metals and radionuclides, Curr. Opin. Biotechnol. 12 (2001) 248–253.
[5] I. Ortiz-Bernad, R.T. Anderson, H.A. Vrionis, D.R. Lovley, Vanadium respiration by *Geobacter metallireducens*: novel strategy for *in situ* removal of vanadium from groundwater, Appl. Environ. Microbiol. 70 (2004) 3091–3095.
[6] J.N. Rooney-Varga, R.T. Anderson, J.L. Fraga, D. Ringelberg, D.R. Lovley, Microbial communities associated with anaerobic benzene degradation in a petroleum-contaminated aquifer, Appl. Environ. Microbiol. 65 (1999) 3056–3063.
[7] Y. Sung, K.E. Fletcher, K.M. Ritalahti, R.P. Apkarian, N. Ramos-Hernandez, R.A. Sanford, N.M. Mesbah, F.E. Loffler, *Geobacter lovleyi* sp. nov. strain SZ, a novel metal-reducing and tetrachloroethene-dechlorinating bacterium, Appl. Environ. Microbiol. 72 (2006) 2775–2782.
[8] S.E. Childers, S. Ciufo, D.R. Lovley, *Geobacter metallireducens* accesses insoluble Fe (III) oxide by chemotaxis, Nature 416 (2002) 767–769.
[9] K.P. Nevin, D.R. Lovley, Mechanisms for Fe(III) oxide reduction in sedimentary environments, Geomicrobiol. J. 19 (2002) 141–159.
[10] K.P. Nevin, D.R. Lovley, Mechanisms for accessing insoluble Fe(III) oxide during dissimilatory Fe(III) reduction by *Geothrix fermentans*, Appl. Environ. Microbiol. 68 (2002) 2294–2299.
[11] B.A. Methe, K.E. Nelson, J.A. Eisen, I.T. Paulsen, W. Nelson, J.F. Heidelberg, D. Wu, M. Wu, N. Ward, M.J. Beanan, R.J. Dodson, R. Madupu, L.M. Brinkac, S.C. Daugherty, R.T. Deboy, A.S. Durkin, M. Gwinn, J.F. Kolonay, S.A. Sullivan, D.H. Haft, J. Selengut, T.M. Davidsen, N. Zafar, O. White, B. Tran, C. Romero, H.A. Forberger, J. Weidman, H. Khouri, T.V. Feldblyum, T.R. Utterback, S.E. Van Aken, D.R. Lovley, C.M. Fraser, Genome of *Geobacter sulfurreducens*: metal reduction in subsurface environments, Science 302 (2003) 1967–1969.
[12] J.E. Butler, N.D. Young, D.R. Lovley, Evolution of electron transfer out of the cell: comparative genomics of six *Geobacter* genomes, BMC Genomics 11 (2010) 40.

[13] M. Aklujkar, J. Krushkal, G. DiBartolo, A. Lapidus, M.L. Land, D.R. Lovley, The genome sequence of *Geobacter metallireducens*: features of metabolism, physiology and regulation common and dissimilar to *Geobacter sulfurreducens*, BMC Microbiol. 9 (2009) 109.
[14] J.R. Lloyd, C. Leang, A.L. Hodges Myerson, M.V. Coppi, S. Ciufo, B. Methe, S.J. Sandler, D.R. Lovley, Biochemical and genetic characterization of PpcA, a periplasmic *c*-type cytochrome in *Geobacter sulfurreducens*, Biochem. J. 369 (2003) 153–161.
[15] J.E. Butler, F. Kaufmann, M.V. Coppi, C. Nunez, D.R. Lovley, MacA, a diheme *c*-type cytochrome involved in Fe(III) reduction by *Geobacter sulfurreducens*, J. Bacteriol. 186 (2004) 4042–4045.
[16] C. Leang, M.V. Coppi, D.R. Lovley, OmcB, a *c*-type polyheme cytochrome, involved in Fe(III) reduction in *Geobacter sulfurreducens*, J. Bacteriol. 185 (2003) 2096–2103.
[17] B.C. Kim, C. Leang, Y.H. Ding, R.H. Glaven, M.V. Coppi, D.R. Lovley, OmcF, a putative *c*-type monoheme outer membrane cytochrome required for the expression of other outer membrane cytochromes in *Geobacter sulfurreducens*, J. Bacteriol. 187 (2005) 4505–4513.
[18] B.C. Kim, X. Qian, C. Leang, M.V. Coppi, D.R. Lovley, Two putative c-type multiheme cytochromes required for the expression of OmcB, an outer membrane protein essential for optimal Fe(III) reduction in *Geobacter sulfurreducens*, J. Bacteriol. 188 (2006) 3138–3142.
[19] B.C. Kim, D.R. Lovley, Investigation of direct vs. indirect involvement of the *c*-type cytochrome MacA in Fe(III) reduction by *Geobacter sulfurreducens*, FEMS Microbiol. Lett. 286 (2008) 39–44.
[20] T. Mehta, M.V. Coppi, S.E. Childers, D.R. Lovley, Outer membrane *c*-type cytochromes required for Fe(III) and Mn(IV) oxide reduction in *Geobacter sulfurreducens*, Appl. Environ. Microbiol. 71 (2005) 8634–8641.
[21] K.P. Nevin, B.C. Kim, R.H. Glaven, J.P. Johnson, T.L. Woodard, B.A. Methe, R.J. DiDonato Jr., S.F. Covalla, A.E. Franks, A. Liu, D.R. Lovley, Anode biofilm transcriptomics reveals outer surface components essential for high density current production in *Geobacter sulfurreducens* fuel cells, PLoS ONE 4 (2009) e5608.
[22] X. Qian, G. Reguera, T. Mester, D.R. Lovley, Evidence that OmcB and OmpB of *Geobacter sulfurreducens* are outer membrane surface proteins, FEMS Microbiol. Lett. 277 (2007) 21–27.
[23] Y.R. Ding, K.K. Hixson, M.A. Aklujkara, M.S. Lipton, R.D. Smith, D.R. Lovley, T. Mester, Proteome of *Geobacter sulfurreducens* grown with Fe(III) oxide or Fe(III) citrate as the electron acceptor, BBA Proteins Proteomics 1784 (2008) 1935–1941.
[24] C. Leang, X. Qian, T. Mester, D.R. Lovley, Alignment of the *c*-type cytochrome OmcS along pili of *Geobacter sulfurreducens*, Appl. Environ. Microbiol. 76 (2010) 4080–4084.
[25] D.E. Holmes, S.K. Chaudhuri, K.P. Nevin, T. Mehta, B.A. Methé, A. Liu, J.E. Ward, T.L. Woodard, J. Webster, D.R. Lovley, Microarray and genetic analysis of electron transfer electrodes in *Geobacter sulfurreducens*, Environ. Microbiol. 8 (2006) 1805–1815.
[26] J.W. Voordeckers, B.C. Kim, M. Izallalen, D.R. Lovley, Role of *Geobacter sulfurreducens* outer-surface *c*-type cytochromes in the reduction of soil humic acid and anthraquinone-2, 6-disulfonate, Appl. Environ. Microbiol. 76 (2010) 2371–2375.
[27] M.V. Coppi, C. Leang, S.J. Sandler, D.R. Lovley, Development of a genetic system for *Geobacter sulfurreducens*, Appl. Environ. Microbiol. 67 (2001) 3180–3187.
[28] S.J. Field, P.S. Dobbin, M.R. Cheesman, N.J. Watmough, A.J. Thomson, D.J. Richardson, Purification and magneto-optical spectroscopic characterization of cytoplasmic membrane and outer membrane multiheme *c*-type cytochromes from *Shewanella frigidimarina* NCIMB400, J. Biol. Chem. 275 (2000) 8515–8522.
[29] G. Bohm, G. Muhr, R. Jaenicke, Quantitative analysis of protein far UV circular dichroism spectra by neural net works, Protein Eng. 5 (1992) 191–195.
[30] L. Morgado, M. Bruix, V. Orshonsky, Y.Y. Londer, N.E. Duke, X. Yang, P.R. Pokkuluri, M. Schiffer, C.A. Salgueiro, Structural insights into the modulation of the redox properties of two *Geobacter sulfurreducens* homologous triheme cytochromes, Biochim. Biophys. Acta 1777 (2008) 1157–1165.
[31] L. Morgado, M. Bruix, M. Pessanha, Y.Y. Londer, C.A. Salgueiro, Thermodynamic characterization of a triheme cytochrome family from *Geobacter sulfurreducens* reveals mechanistic and functional diversity, Biophys. J. 99 (2010) 293–301.
[32] H. Zhu, M. Hargrove, Q. Xie, Y. Nozaki, K. Linse, S.S. Smith, J.S. Olson, A.F. Riggs, Stoichiometry of subunits and heme content of hemoglobin from the earthworm *Lumbricus terrestris*, J. Biol. Chem. 271 (1996) 29999–30006.
[33] L. Pieulle, J. Haladjian, J. Bonicel, E.C. Hatchikian, Biochemical studies of the *c*-type cytochromes of the sulfate reducer *Desulfovibrio africanus*. Characterization of two tetraheme cytochromes c_3 with different specificity, BBA-Bioenergetics 1273 (1996) 51–61.
[34] G.R. Moore, G.W. Pettigrew, Cytochromes *c*: Evolutionary, Structural and Physicochemical Aspects, Springer-Verlag, Berlin, 1990.
[35] N. Greenfield, G.D. Fasman, Computed circular dichroism spectra for the evaluation of protein conformation, Biochemistry 8 (1969) 4108–4116.
[36] I. Bertini, C. Luchinat, NMR of Paramagnetic Molecules in Biological Systems, Benjamin/Cummings, Menlo Park, CA, 1986.
[37] C.C. McDonald, W.D. Phillips, S.N. Vinogradov, Proton magnetic resonance evidence for methionine-iron coordination in mammalian-type ferrocytochrome *c*, Biochem. Biophys. Res. Commun. 36 (1969) 442–449.
[38] D.R. Lovley, D.E. Holmes, K.P. Nevin, Dissimilatory Fe(III) and Mn(IV) reduction, Adv. Microb. Physiol. 49 (2004) 219–286.
[39] F. Caccavo, D.J. Lonergan, D.R. Lovley, M. Davis, J.F. Stolz, M.J. Mclnerney, *Geobacter sulfurreducens* sp. nov., a hydrogen- and acetate-oxidizing dissimilatory metal-reducing microorganism, Appl. Environ. Microbiol. 60 (1994) 3752–3759.
[40] D.R. Lovley, E.J.P. Phillips, Bioremediation of uranium contamination with enzymatic uranium reduction, Environ. Sci. Technol. 26 (1992) 2228–2234.
[41] D.R. Lovley, Dissimilatory metal reduction, Annu. Rev. Microbiol. 47 (1993) 263–290.
[42] D.R. Lovley, J.D. Coates, E.L. Blunt-Harris, E.J.P. Phillips, J.C. Woodward, Humic substances as electron acceptors for microbial respiration, Nature 382 (1996) 445–447.
[43] Z. Wang, C. Liu, X. Wang, M.J. Marshall, J.M. Zachara, K.M. Rosso, M. Dupuis, J.K. Fredrickson, S. Heald, S. Liang, Kinetics of reduction of Fe(III) complexes by outer membrane cytochromes MtrC and OmcA of *Shewanella oneidensis* MR-1, Appl. Environ. Microbiol. 74 (2008) 6746–6755.
[44] M.E. Hernandez, D.K. Newman, Extracellular electron transfer, Cell. Mol. Life Sci. 58 (2001) 1562–1571.
[45] R.S. Hartshorne, B.N. Jepson, T.A. Clarke, S.J. Field, J. Fredrickson, J. Zachara, L. Shi, J.N. Butt, D.J. Richardson, Characterization of *Shewanella oneidensis* MtrC: a cell-surface decaheme cytochrome involved in respiratory electron transport to extracellular electron acceptors, J. Biol. Inorg. Chem. 12 (2007) 1083–1094.
[46] N.S. Wigginton, K.M. Rosso, M.F. Hochella Jr., Mechanisms of electron transfer in two decaheme cytochromes from a metal-reducing bacterium, J. Phys. Chem. B 111 (2007) 12857–12864.
[47] D. Leys, T.E. Meyer, A.S. Tsapin, K.H. Nealson, M.A. Cusanovich, J.J. Van Beeumen, Crystal structures at atomic resolution reveal the novel concept of "electron-harvesting" as a role for the small tetraheme cytochrome *c*, J. Biol. Chem. 277 (2002) 35703–35711.
[48] K. Inouye, T. Mizokawa, A. Saito, B. Tonomura, H. Ohkawa, Biphasic kinetic behavior of rat cytochrome P-4501A1-dependent monooxygenation in recombinant yeast microsomes, Biochim. Biophys. Acta 1481 (2000) 265–272.
[49] K. Inoue, X. Qian, L. Morgado, B.C. Kim, T. Mester, M. Izallalen, C.A. Salgueiro, D.R. Lovley, Purification and characterization of OmcZ, an outer-surface, octaheme *c*-type cytochrome essential for optimal current production by *Geobacter sulfurreducens*, Appl. Environ. Microbiol. 76 (2010) 3999–4007.